Chapter 3
Fundamentals of Laser-Material Interactions

Ettore Carpene, Daniel Höche, and Peter Schaaf

Abstract The following chapter illustrates the basic physical processes occurring during laser-material interaction. It considers fundamentals of electrodynamics in relation to electron–phonon interaction, electromagnetic wave propagation and phase transformations that take place. The theory explains the influence of interaction times and their consequences on heat and material transport.

3.1 Basic Considerations

Laser-material interactions are very complex and only in some simple cases, the laser may be merely seen as a heat source. The numerous facets of laser-material coupling have been the focus of physical research immediately after the first operating laser was built [1–8]. Absorption, heating, melting, evaporation, recoil pressure, piston effect, plasma formation, laser-supported absorption waves (LSAW), Marangoni convection, and Kelvin-Helmholtz instabilities are among the intricate aspects of the laser-material interaction, and they all should be taken into account in order to understand in details the effects of laser processing on the irradiated substrate.

In this chapter, we give a short overview on some of the main features of common types of lasers (Sect. 3.2), sketch the basic electron–electron and electron-lattice dynamics related to laser-material coupling (Sect. 3.3), discuss the fundamental aspects of laser-material interaction (Sect. 3.4.1) with connection to the thermophysical properties of the substrate (Sect. 3.4.2), and show the results of numerical simulations on some common materials (Sect. 3.4.3). In Sect. 3.5, we give an overview of the phenomena occurring at the sample surface during energetic pulsed laser processing: in particular evaporation (Sect. 3.5.1), recondensation (Sect. 3.5.2), plasma formation (Sect. 3.5.3), and LSAW (Sect. 3.5.4) will be outlined. We will conclude sketching some basic aspects of material transport processes (Sect. 3.6).

E. Carpene (✉)
CNR-IFN, Dipartimento di Fisica, Politecnico di Milano, piazza Leonardo da Vinci 32, 20133 Milano, Italy
e-mail: ettore.carpene@fisi.polimi.it

3.2 Laser

It took many years since the publication of the basic theoretical principles of the stimulated emission of radiation by Einstein in 1917 [9] until the first radiating laser was built by Maiman in 1960 [10]. With the development of powerful lasers, also their applications in material treatments rapidly developed [11–16]. Today, an uncountable number of lasers are used in industrial production processes, especially for the treatment of metals.

A laser (**LASER** = **L**ight **A**mplification by **S**timulated **E**mission of **R**adiation) is a device that emits light (i.e., electromagnetic radiation) through the process of stimulated emission. The basic principles of a laser are described in [17–20]. One can classify lasers into the following types, according to the lasing medium:

1. Gas lasers (e.g., CO_2, excimer)
2. Liquid lasers (organic liquid dye)
3. Solid state lasers (e.g., Nd-YAG, Ti:sapphire, fibre laser)
4. Semiconductor laser (e.g., quantum cascade lasers, diode laser)
5. Free electron laser (FEL)

A laser can radiate either in continuous wave (cw) mode or in pulsed mode. The first operating laser was a Ruby laser [10], i.e., a solid state laser. Here, the population inversion was produced by optical pumping. Semiconductor lasers are using a voltage/current to invert the state occupancy, while in gas laser the inversion is obtained by gas discharge. In particular, the excimer laser (excimer=excited dimer) is a pulsed, high pressure gas laser, using a noble gas – halogen mixture [21]. FELs use relativistic electrons as lasing medium and they provide the widest spectral tunability (form far IR to deep UV or soft X-rays). The main properties of laser radiation are the high brightness (i.e., power emitted per unit surface area per unit solid angle), high monochromaticity (i.e., extremely narrow bandwidth), minimal divergence, and high spatial and temporal coherence [3, 22]. These are the reasons for the high focussability of laser radiation, which leads to the production of large irradiances (up to 10^{21} W/cm^2), enough to evaporate any material or even to start a nuclear fusion reaction [17]. The temporal structure of pulsed lasers depends on the specific lasing process, but it can range from milliseconds to femtosecond with the mode-locking technique. The spatial energy distribution in the laser beam is mainly depending on the geometry of the laser resonator, on the mirrors and on the extraction optics [23, 24]. Best focussability is given at low transversal electromagnetic radiation modes (TEM00, i.e., Gaussian), whereas for surface treatments a top-hat profile is preferred in order to achieve a homogeneous treatment. The most important lasers for material treatments are the CO_2 laser, the Nd:YAG laser, and the excimer laser. Recently, also diode lasers are attracting great interest [25]. For laser processing of metals, the beam wavelength is relatively important as long as light is absorbed. For dielectric materials, on the other hand, considerable absorption takes place only if the photon energy overcomes the optical/mobility gap.

The typical wavelengths λ of various laser types are summarized in Table 3.1 [26].

Table 3.1 Wavelengths for selected laser types [26]

Lasing medium	Laser type	Wavelength
Solid-state	Ruby	694 nm
	Nd:YAG	1,064 nm
	Ti:Sapphire	650–1,100 nm
Gas	CO_2	10.4 μm
	Excimer	193 nm (Ar–F)
		248 nm (Kr–F)
		308 nm (Xe–Cl)
		351 nm (Xe–F)
Semiconductor	GaN	0.4 μm
	Quantum cascade	mid-far IR
Free electron		far IR to vacuum UV

For laser processing of solid substrates, the typical power of the laser beam is ranging up to 100 MW with pulse durations τ_{pulse} of 10–100 ns and repetition rates up to 1 kHz [20, 26, 27].

3.3 Heat in Solids: Electronic and Lattice Dynamics

To understand the effect of the laser beam on the irradiated material, the electronic and lattice dynamics must be taken into account. In order to induce any effect on the substrate, the laser light must be absorbed and the absorption process can be thought as an energy source inside the material. However, although driven by the incident light beam, the source can develop its own dynamics depending on the specific electronics and lattice responses of the material. The description of the absorption phenomena is based on Maxwell's equations and on their solution for time-varying electric and magnetic fields. The optical properties of solids are accessible with conventional optical methods using light in the infrared, visible, and ultraviolet spectral range. In this section, we summarize the basic electronic and lattice dynamics of solids, emphasizing their typical time scales and their consequences on the laser-material interaction.

For typical laser wavelengths (from near infrared to near ultraviolet), photons are absorbed by electrons through inter- and intra-band electronic transitions. Therefore, the laser beam induces a non-equilibrium electronic distribution that thermalizes via electron–electron and electron–phonon interactions. The electron–electron thermalization can be rather complex depending on the specific electronic structure of the irradiated sample: for semiconductors and insulators, the laser photons can promote electrons from the valence band to the conduction band, across the optical/mobility gap, creating electron-hole pairs. Subsequently, electronic recombination reestablishes the equilibrium condition on a time scale that can be as long as nanoseconds, depending on the material properties [28].

For metals, the situation can be very different. Electron scattering events can take place within a few femtoseconds, thus electronic thermalization can be extremely fast. The simplest approach is provided by the Drude model [29], where the electron scattering time τ_D can be deduced from the electrical conductivity σ_{el} as:

$$\sigma_{el} = Ne^2\tau_D/m \tag{3.1}$$

Here, N is the conduction electron density, e is the electron charge, and m is the electron mass. Typical values of τ_D are a few femtoseconds, representing the time scale of electron scattering events. Drude model simply provides the electron scattering time even under equilibrium conditions, with no insight on the specific mechanism. Since the laser photons induce a non-equilibrium electronic distribution, more sophisticated approaches must be employed. The lifetime τ_{ee} of excited electron is due to electron–electron collisions and is described by the Fermi liquid theory [30] as:

$$\tau_{ee} = \tau_0 \left(\frac{\varepsilon_F}{\varepsilon - \varepsilon_F} \right)^2 \tag{3.2}$$

where τ_0 is of the order of a femtosecond, ε_F is the Fermi energy, and $\varepsilon - \varepsilon_F$ is the excited electron energy as referred to the Fermi level. Notice that with laser photons in the visible-UV range and with a typical Fermi energy of 10 eV, $\tau_{ee} \sim 1 - 10$ fs and it rapidly increases as the electron energy relaxes towards the Fermi level. This lifetime dependence has been thoroughly investigated and confirmed by several time-resolved photoemission experiments using femtosecond lasers (see for instance [31, 32]). Due to the ultrafast character of electron–electron interaction, these processes can only be revealed with laser pulses which duration compares with τ_{ee}, i.e., Ti:sapphire lasers operating in mode-locking condition. For longer laser pulses, the electron–electron thermalization occurs *within* the pulse duration and the electron dynamics substantially follows the time evolution of the laser pulse.

Electrons, however, do not only scatter among each other, but they can also interact with the lattice through electron–phonon scattering processes. The theory of electron-lattice scattering has been developed since the 1960s, especially with the discovery of superconductivity. The basic features of the interaction have been outlined in the fundamental work of Eliashberg (see [33]). A simplified approach, directly related to laser interaction with solid has been proposed by P. B. Allen [34], and is based on the rate of change of the electron and phonon distributions due to collisions. Allen derived an expression for the energy transfer between the photo-excited electrons and the lattice that allows to evaluate the variation of the electronic temperature T_e as a simple rate equation:

$$\partial T_e/\partial t = (T_L - T_e)/\tau_{ep} \tag{3.3}$$

(T_L is the lattice temperature) where the electron–phonon coupling time τ_{ep} depends on the electronic temperature, a coupling constant λ_p (~ 0.5, see [35]) characteristic of the material and the Debye frequency ω_D of the irradiated solid as:

$$\tau_{ep} = (2\pi k_B T_e)/(3\hbar\lambda_p\omega_D^2) \tag{3.4}$$

For $T_e \sim 10^3$ K and using typical values of the Debye frequency for metals ($\hbar\omega_D$ of a few tens of meV), $\tau_{ep} \sim 0.1-1$ ps. Thus, the energy transfer from the electronic bath to the lattice occurs on the picosecond time scale and is roughly two orders of magnitude slower than the electron–electron scattering time.

From these considerations, it is clear that electrons and lattice can develop distinct dynamics upon laser irradiation, and the time evolution of the energy (or temperature) of the electron gas and the lattice can be described by two separate, but coupled heat transport equations:

$$C_e \frac{\partial T_e}{\partial t} = \nabla(k_e \nabla T_e) - H(T_e, T_L) + S(t) \tag{3.5}$$

$$C_L \frac{\partial T_L}{\partial t} = H(T_e, T_L) \tag{3.6}$$

Here, C_e and C_L are the electronic and lattice specific heat (J m^{-3} K^{-1}), respectively, $S(t)$ represents the absorbed laser power per unit volume (W m^{-3}), $H(T_e, T_L)$ is the rate of energy transfer between electrons and lattice (W m^{-3}), and $\nabla(k_e \nabla T_e)$ is the diffusive electronic heat transfer. These coupled differential equations represent the celebrated two-temperature model (TTM) developed by Anisimov et al. in 1975 [36]. In the last 30 years, several authors have investigated theoretically and experimentally various aspects on the TTM, including the detailed electronic [37–45] and spin [46] scattering mechanisms.

Under proper experimental conditions (see [38,47]), the energy transfer between electrons and lattice can be simplified as:

$$H(T_e, T_L) = g_{ep}(T_L - T_e) \tag{3.7}$$

where the quantity $g_{ep} = C_e/\tau_{ep}$ represents an alternative way (but equivalent to the approach proposed by Allen) to describe the electron–phonon coupling.

It should be noted that (3.5) and (3.6) are useful as long as the laser pulse duration τ_{pulse} is comparable to the typical time constants of electron–electron and electron–phonon couplings. If $\tau_{pulse} \gg \tau_{ee}, \tau_{ep}$, then electrons and lattice thermalize within the pulse duration and their dynamics substantially coincide (thus $T_e = T_L = T$). To illustrate this effect, (3.5) and (3.6) have been solved numerically (details on the numerical simulation of the temperature profiles will be discussed in Sect. 3.4.3) using the thermal and optical parameters of copper as a benchmark. The temporal profiles of the source term $S(t)$ has been assumed gaussian and the laser fluence has been chosen for each pulse duration in order to produce a maximum electronic temperature rise $\Delta T < 100$ K. For copper, $C_e = \gamma T_e$, with $\gamma = 10^{-4}$ J/cm^{3}K^2 [48], $C_L = 3.4$ J/cm^{3}K [48], $k_e = 4$ W/(cm K) [49] and $g_{ep} = 10^{10}$ W/cm^3 K [49], corresponding to an electron–phonon coupling time $\tau_{ep} \sim 0.3$ ps. The results are reported in Fig. 3.1.

For $\tau_{pulse} = 50$ fs, electrons and lattice are essentially decoupled: the electronic temperature rise is determined by the laser pulse and its subsequent relaxation is completed on a time scale comparable to a few τ_{ep}. The lattice temperature, on the

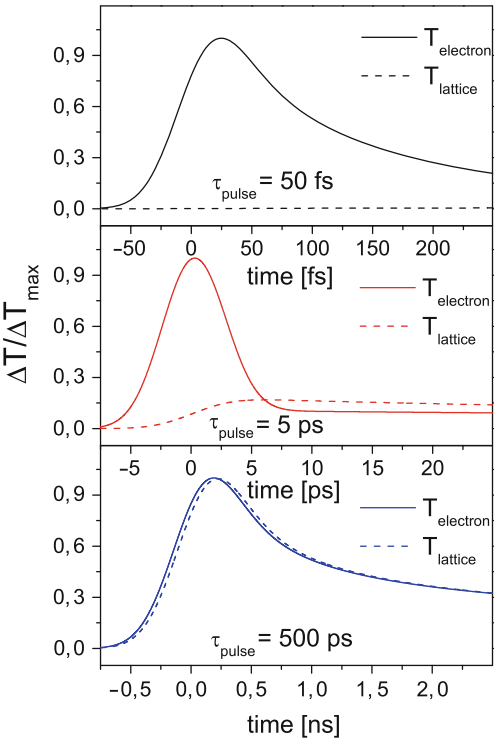

Fig. 3.1 Electronic and lattice temperature profiles (simulations obtained with the TTM) in cupper irradiated by laser pulses of different durations (ranging from 50 fs to 500 ps). With 50 fs pulses, electrons and lattice are completely decoupled and the lattice is substantially unaffected by the laser beam. With 500 ps pulses, electron and lattice follow almost identical temperature evolutions

other hand, shows a negligible change since the lattice cannot respond on a time scale as short as the pulse duration. When $\tau_{\text{pulse}} = 5$ ps, the electronic temperature closely resemble the time evolution of the laser pulse (i.e., gaussian profile) since its intrinsic dynamics is much faster than τ_{pulse}. Besides, energy is transferred to the lattice within the pulse duration and T_{L} clearly rises. If the laser pulse duration is further increased to $\tau_{\text{pulse}} = 500$ ps, electronic and lattice dynamics are essentially similar since the rate of energy exchange between them is much shorter than τ_{pulse} and they evolve as if they were in local thermal equilibrium condition.

In this last case, the TTM becomes redundant, and (3.5) and (3.6) can be simplified. In fact, by substituting (3.6) in (3.5) one obtains:

$$(C_{\text{e}} + C_{\text{L}})\frac{\partial T}{\partial t} = \nabla(k_{\text{e}}\nabla T) + S(t) \tag{3.8}$$

Considering that the electronic specific heat is usually much smaller than the lattice one [29, 48], the term C_{e} can be neglected and the standard heat transport equation is obtained:

$$C_{\text{L}}\frac{\partial T}{\partial t} = \nabla(k_{\text{e}}\nabla T) + S(t) \tag{3.9}$$

The main features and the most important consequences of this equation will be described in detail in the next sections.

3.4 Laser-Material Interactions

The laser is usually seen as a very special and intense heat source and only its thermal effects are to be considered. Nevertheless, in recent years also laser induced chemical reactions, where photons with high enough energy may directly induce chemical reactions, play a considerable role [1, 7].

Even if the laser processing is performed in the presence of a reactive atmospheric environment (e.g., nitrogen or methane for laser-induced nitriding and carburizing, respectively), photon energy in the near UV spectral range is too small to directly interact with the surrounding gas with typical ionization energy of tens of eV (e.g., $E_{\text{ioniz}} = 15.6\,\text{eV}$ for nitrogen [50]). Moreover, the intensity of the laser irradiation normally used in laser processing of matter is too small to induce a gas breakdown, which needs a threshold irradiance of $I_{\text{break}} \approx 10^{10}\,\text{W/cm}^2$ [1, 51]. Thus, the laser irradiation will hit the substrate surface unhindered, without absorption in the surrounding gas.

3.4.1 Single Photon and Multi-Photon Processes

The processes taking place when the laser radiation hits a material depend on the amount of deposited laser energy. This energy and its spatial and temporal distribution determine what kind of material modification will occurs [52]. The main laser-solid interaction process is the excitation of electrons from their equilibrium states to some excited states by absorption of photons [53]. These typical single photon processes are well-known in a wide field of physics and have been discussed extensively [54, 55]. Other possible excitations involve multiphoton electronic transitions. At a constant laser fluence, a shorter laser-material interaction time favors multiphoton excitation processes, because the probability of nonlinear absorption increases strongly with a growing laser intensity.

A general expression for the n-photon transition probability W is given by the following equation:

$$W = s^n I^n \tag{3.10}$$

where I describes the laser intensity and s the cross section of the single-photon process. Due to their strong nonlinear character, multiphoton processes are in general rather complex and will not be considered in the next sections. Further information are available in the work of Linde et al. [53].

3.4.2 Laser Reflection and Absorption

As already mentioned in previous chapters, laser light in the near IR-near UV spectral region normally interacts only with the electrons of a material, because ions are too heavy to follow the high frequency fields [56]. The optical properties of metals are determined by the free (valence) electrons, because the inner electrons only weakly interact with the applied electric field. These free electrons are accelerated in the electrical field and gain energy. Due to the periodic change of the field vector, the oscillating electrons also re-radiate energy, which causes the high reflectivity of metals. The interactions of laser radiation with matter are significantly simplified if the pulse duration is long compared to the typical elementary scattering times (picoseconds), and the classical Drude theory [57] can be used.

Describing the laser radiation by a propagating electric field plane wave:

$$\mathbf{E}(\mathbf{r},t) = \mathbf{E_0} \exp\{\,\mathrm{i}\,(\mathbf{kr} - \omega t)\,\} \tag{3.11}$$

with frequency $\omega = 2\pi c/\lambda$, wavevector $\mathbf{k}$, space coordinate $\mathbf{r}$, time t, and field amplitude $\mathbf{E}_0$, one can treat the solid as a combination of harmonic oscillators (Lorentz model), resulting in the equation of motion for electrons:

$$m\ddot{\mathbf{r}} + m\gamma_\mathrm{D}\dot{\mathbf{r}} + m\omega_0^2\mathbf{r} = -e\mathbf{E}_\mathrm{loc}(\mathbf{r},t) \tag{3.12}$$

with electron mass m, attenuation $\gamma_\mathrm{D} = 1/\tau_\mathrm{D}$, eigenfrequency ω_0 and the local field strength $\mathbf{E}_\mathrm{loc}$.

Here the finite mass of the atoms and the weak magnetic forces have been neglected. The attenuation constant γ_D includes the interaction of the electrons with lattice phonons and vacancies, by which energy is transferred within picoseconds to the whole solid [8]. The fraction of absorbed radiation is determined by the optical properties of the sample. The locally acting electric field $\mathbf{E}_\mathrm{int} = \langle\mathbf{E}_\mathrm{loc}\rangle$ is the response of the material to the external field and is determined by the dielectric tensor ε via:

$$\mathbf{E_0} = \varepsilon \cdot \mathbf{E}_\mathrm{int} \tag{3.13}$$

For isotropic materials, the dielectric tensor reduces to a complex constant and in the framework of the Drude model for metal, considering that free electrons have no retention force, i.e., $\omega_0 = 0$, the dielectric index $\varepsilon = \varepsilon_1 + \mathrm{i}\,\varepsilon_2$ is given by:

$$\varepsilon_1 = n^2 - \kappa^2 = 1 - \frac{\omega_\mathrm{p}^2\tau_\mathrm{D}^2}{1+\omega^2\tau_\mathrm{D}^2} \tag{3.14}$$

$$\varepsilon_2 = 2n\kappa = \frac{\omega_\mathrm{p}^2\tau_\mathrm{D}}{\omega(1+\omega^2\tau_\mathrm{D}^2)}, \tag{3.15}$$

with n and κ being the so-called refractive index and the extinction coefficient. As already discussed, τ_D is the mean time between two electronic collisions. The plasma frequency ω_p depends on density of free electrons N:

$$\omega_\mathrm{p} = \sqrt{\frac{Ne^2}{m\varepsilon_0}} \tag{3.16}$$

(here, ε_0 is the vacuum dielectric constant). The reflectivity R_0 and the absorption coefficient α, or the optical absorption length $d_\mathrm{opt} = 1/\alpha$ (at normal incidence), may be obtained via n and κ by:

$$R_0 = \frac{(n-1)^2 + \kappa^2}{(n+1)^2 + \kappa^2} \tag{3.17}$$

$$\alpha = \frac{2\omega\kappa}{c} = \frac{4\pi\kappa}{\lambda} \tag{3.18}$$

Simultaneously, the plasma frequency ω_p is connected to the electrical conductivity of the metal σ_el:

$$\sigma_\mathrm{el} = \frac{Ne^2\tau_\mathrm{D}}{m} = \omega_\mathrm{p}^2\tau_\mathrm{D}\varepsilon_0 \tag{3.19}$$

and is usually in the UV regime.

For optical wavelengths $\omega \ll 1/\tau_\mathrm{D}$ (IR spectral range), the reflectivity R_0 and the absorption coefficient α can be estimated using the electrical resistivity $\rho_\mathrm{el} = 1/\sigma_\mathrm{el}$ (Hagen-Rubens-equation [56, 58]):

$$R_0 = 1 - 2\sqrt{2\omega\varepsilon_0\rho_\mathrm{el}} \tag{3.20}$$

$$\alpha = \sqrt{\frac{2\omega}{c^2\varepsilon_0\rho_\mathrm{el}}} \tag{3.21}$$

resulting in $R_0 \approx 90 - 99\%$, and $\alpha^{-1} \approx 10\,\mathrm{nm}$ for metals and radiation below the plasma frequency [56]. The absorption coefficient increases with decreasing wavelength and is proportional to the resistivity ρ_el [59], while above the plasma frequency the reflectivity drops drastically (UV-transparency of metals) [60]. The values of R_0 and α, or alternatively n and κ, are available in the literature for many pure solids and for a number of compounds in a wide range of laser wavelengths [50, 61].

The absorption at surfaces not only depends on the wavelength of the laser radiation, but also on other factors such as incident angle, surface roughness, and temperature of the solid. For example, the roughening of the surface (roughness $R_\mathrm{a} > \lambda$) enhances the absorption by multiple reflections [59]. For most metals, the absorption increases with increasing surface temperature. A dramatic increase of the absorption is found for most metals at the melting point [56]. Also for high enough laser intensities (10^5–$10^6\,\mathrm{W/cm^2}$), anomalous absorption by nonlinear processes can enhance the energy transfer [19, 62].

As stated by (3.9), the absorbed energy is spatially distributed by heat conduction. For laser with pulse duration up to tens of nanoseconds, the thermal diffusion length z_th never exceeds a few µm (for metals $z_\mathrm{th} = \sqrt{\tau_\mathrm{pulse}k_\mathrm{e}/C_\mathrm{L}} < 1\,\mu\mathrm{m}$, where

k_e/C_L is the so-called thermal diffusivity). Assuming a laser spot size much larger than the thermal diffusion length z_{th} (that is a rather common situation in standard laser processing), one can use the one-dimensional heat diffusion equation, and (3.9) can be further simplified. For the isotropic case with temperature dependent material properties, this can be written as:

$$C_L(T)\frac{\partial T(z,t)}{\partial t} = \frac{\partial}{\partial z}\left[k_e(T)\frac{\partial T(z,t)}{\partial z}\right] + S(z,t), \tag{3.22}$$

where $T(z,t)$ is the temperature at depth z at time t; $\zeta = \frac{k_e(T)}{C_L}$, where $k_e(T)$ is the heat conductivity, $C_L(T)$ is the specific heat and $S(z,t)$ is the absorbed or released energy per unit time and unit volume.

Here, $S(z,t)$ incorporates the laser heat sources, i.e., the absorbed laser energy $I_{abs}(z,t)$, as well as internal heat sinks $\Delta U(z,t)$ due to phase transformation:

$$S(z,t) = I_{abs}(z,t) + \Delta U(z,t) \tag{3.23}$$

The absorbed laser energy can be evaluated using the laser *irradiance* $I(t)$ (i.e., energy per unit area and unit time), the reflectivity R_0 and the absorption coefficient α:

$$I_{abs} = I(t)\alpha(1 - R_0)\exp(-\alpha z)\,. \tag{3.24}$$

that is a direct consequence of Beer's law:

$$\frac{\partial I(t,z)}{\partial z} = -\alpha I(t,z). \tag{3.25}$$

The temporal shape of the laser beam can be modeled according to the laser specification, but it is customary to use a Gaussian profile:

$$I(t) = (\phi/\sigma\sqrt{2\pi}) \cdot \exp(-(t - t_0)^2/2\sigma^2). \tag{3.26}$$

where ϕ is the laser *fluence* (i.e., energy per unit area) and $\tau_{pulse} = 2\sigma\sqrt{\ln 2}$ (i.e., the FWFM of the gaussian profile).

When a phase transformation occurs (e.g., melting, evaporation, or solidification) at a given temperature T_{phase}, the corresponding latent heat L_{phase} is a heat sink that must be taken into account. A convenient approach is to re-define heat in the proximity of the phase transition temperature in such a way that uniquely describes the state of the material as a function of the temperature [28]:

$$\mathrm{d}H(T) = \begin{cases} C_L \mathrm{d}T & \text{if } T < T_{phase}; \\ C_L \mathrm{d}T + L_{phase} & \text{if } T \geq T_{phase}. \end{cases} \tag{3.27}$$

When the material changes phase, the extra heat sink L_{heat} is "automatically" included in the heat equation.

If the temperature overcomes the melting point, significant evaporation might start, and this must be carefully included into the calculation, because evaporation not only removes heat but also matter. Above the melting temperature, the liquified matter evaporates according to the following evaporation flux j_{ev} [8, 63]:

$$j_{ev} = \rho \frac{\partial z_{ev}}{\partial t} = \frac{p_D(T)}{\sqrt{(2\pi k_B T / M_a)}} \tag{3.28}$$

where $p_D(T)$ is the vapor pressure of the material at temperature T, M_a is the atomic mass, and ρ is the material density. Boiling is neglected, since the high recoil pressure and the plasma pressure, as we will see later, are increasing the boiling temperature.

The vapor pressure p_D can be described by the Clausius-Clapeyron equation:

$$p_D(T) = p_0 \exp\left[-\frac{\Lambda_b}{R}\left(\frac{1}{T} - \frac{1}{T_b}\right)\right] \tag{3.29}$$

with p_0 being the initial pressure (before evaporation starts), Λ_b the molar latent heat of boiling, T_b the boiling temperature, and R the gas constant. Then, the heat flux U_{ev} removed by the evaporation process is given by

$$U_{ev} = j_{ev}\Lambda_b(T)/M = \rho \frac{\partial z_{ev}}{\partial t} \cdot \Lambda_b(T)/M. \tag{3.30}$$

(M is the molar mass). Since the sample surface is a discontinuity, it requires a boundary condition for the heat diffusion, and it can be included as follows:

$$k_e(T)\left.\frac{\partial T}{\partial z}\right|_{surface} = U_{ev} = \left.\left(\frac{\Lambda_b p_0}{\sqrt{2\pi R T M}} \exp\left[\frac{\Lambda_b}{R}\left(\frac{1}{T_b} - \frac{1}{T}\right)\right]\right)\right|_{surface}. \tag{3.31}$$

As it will be shown in the next sections, during the laser irradiation, an enormous pressure ($\sim 10^2$ bar) is acting on the target surface. According to 3.29, the boiling point is shifted to a higher temperature and the liquid can be heated above T_b, making the condition described in (3.27) unnecessary for the liquid–vapor phase transition.

In most general cases, the thermal and optical parameters appearing in (3.22)–(3.31) are temperature-dependent and the only way to solve the heat transport equation is numerically, as it will be illustrated in the following section with some specific examples.

3.4.3 Temperature Profiles

In this section, we will outline how numerical calculations of the laser induced temperature rise can be performed by the method of finite differences. Due to the fast

and local supply of energy from the laser source, the irradiated sample can melt and even evaporate. The latter is normally connected to the formation of a plasma above the surface. The dependence of temperature, melt depth and evaporation rate on time, depth, and laser fluence will be calculated. Material transport and convection in the melt are neglected at this stage.

In the finite differences approach, time t and space z are divided into discrete points $t^i = i \cdot \Delta t$ and $z_n = n \cdot \Delta z$. Thus, the sample is sliced into thin layers z_n ($n = 0 \ldots N$) of equal distance Δz and the time steps are Δt. The partial time derivative of the temperature can be expressed by the finite difference (forward differentiation) representation:

$$\frac{\partial T}{\partial t} = \frac{T_n^{i+1} - T_n^i}{\Delta t}, \tag{3.32}$$

where T_n^i is the temperature at the time $t^i = i \cdot \Delta t$ in the layer $z_n = n \cdot \Delta z$. The calculation starts at $i = 0$ with $T_n^0 = 300\,\mathrm{K}$ (ambient temperature) for all n. The second derivative in space can also be expressed by a finite difference as:

$$\frac{\partial^2 T}{\partial z^2} = \frac{T_{n-1} - 2T_n + T_{n+1}}{(\Delta z)^2} \tag{3.33}$$

therefore, (3.22) can be re-written as

$$T_n^{i+1} = T_n^i + \Delta t \cdot \left[\frac{k_\mathrm{e}(T_n^i)}{C_\mathrm{L}(T_n^i)} \cdot \frac{(T_{n-1}^i - 2T_n^i + T_{n+1}^i)}{(\Delta z)^2} + \frac{S_n^i}{C_\mathrm{L}(T_n^i)} \right] \tag{3.34}$$

which is called the "forward time centered" space scheme. The source term S_n^i is simply re-written from (3.24)–(3.26) in terms of discrete time and depth.

Also the boundary condition of (3.31) is included in the surface layer ($n = 1$):

$$k_\mathrm{e}(T) \frac{\partial T}{\partial z}\bigg|_\mathrm{surface} = k_\mathrm{e}(T_2^i) \frac{T_2^i - T_1^i}{\Delta z} = \frac{\Lambda_\mathrm{b} p_0}{\sqrt{2\pi R T_1^i M}} \exp\left[\frac{\Lambda_\mathrm{b}}{R} \left(\frac{1}{T_\mathrm{b}} - \frac{1}{T_1^i} \right) \right]. \tag{3.35}$$

Melting and solidification are implemented in the computation via (3.27) by checking for every given layer n at any given time i when the melting point T_m is reached, i.e., $T_n^{i+1} \geq T_\mathrm{m} \geq T_n^i$. If the amount of heat $\Delta H = C_\mathrm{L}(T_n^i)(T_n^{i+1} - T_\mathrm{m}) \leq L_\mathrm{m}$, the layer n starts to melt, the new temperature is held to $T_n^{i+1} = T_\mathrm{m}$ and the fraction $\Delta H / L_\mathrm{m}$ of the slab is molten. On the other hand, if $\Delta H = C_\mathrm{L}(T_n^i)(T_n^{i+1} - T_\mathrm{m}) > L_\mathrm{m}$ the whole slab is molten and the extra heat $\Delta H - L_\mathrm{m} = C_\mathrm{L}(T_n^i)(T_n^{i+1} - T_\mathrm{m})$ determines the temperature T_n^{i+1} of the melt. The solidification process is computed in a similar way.

The heat equation in finite differences becomes an algebraic equation that can be solved with respect to T_n^{i+1}: the temperature is calculated iteratively for each layer at each time step. The values of Δz and Δt are not arbitrarily chosen, but they must satisfy the Neumann criterion [64]:

$$\Delta t < \Delta z^2 \left[\frac{C_{\mathrm{L}}(T)}{2k_{\mathrm{e}}(T)} \right]_{\mathrm{minimum}}, \tag{3.36}$$

in order to obtain convergent, physical solutions. All these details can be implemented into a program running on a standard PC which calculates the temperature profile, the molten depth, and the evaporation rate [65–69].

The simulations presented below refer to a XeCl excimer laser source ($\lambda = 308\,\mathrm{nm}$, $\tau_{\mathrm{pulse}} = 55\,\mathrm{ns}$).

Table 3.2 reports the thermal and optical parameters of Fe, Al, and Si used in the thermal calculations, while Fig. 3.2 shows the temperature dependence of the thermal conductivity $k_{\mathrm{e}}(T)$ and the molar specific heat $c_{\mathrm{p}}(T)$ for pure iron, aluminum, and silicon. Figure 3.3 reports the time evolution of the surface temperature profiles T_1^i and the melting depths of the iron and the aluminum targets irradiated at a laser fluence $\phi = 4\,\mathrm{J/cm^2}$. Considering the typical thermal parameters of the investigated materials, the values of $\Delta z \sim 10\,\mathrm{nm}$ and $\Delta t \sim 1\,\mathrm{ps}$ have been used.

Although it is known that the optical reflectivity R_0 of metals decreases with increasing temperature [28], due to the lack of experimental data, it is assumed

Table 3.2 Thermal and optical parameters of iron, aluminum and silicon used in the heat equation (data from [50])

	Fe	Al	Si
M [g/mole]	56	27	28
ρ [g/cm^3]	7.86	2.7	2.33
L_{m} [kJ/mole]	15	10.5	49.8
L_{ev} [kJ/mole]	350	296	420
T_{m} [K]	1,810	933.5	1,685
T_{b} [K]	3,023	2,740	2,628
R_0 ($\lambda = 308\,\mathrm{nm}$)	0.53	0.5$^{(a)}$	0.6
α [cm^{-1}] ($\lambda = 308\,\mathrm{nm}$)	1×10^6	1.5×10^6	1.5×10^6

$^{(a)}$ Measured.

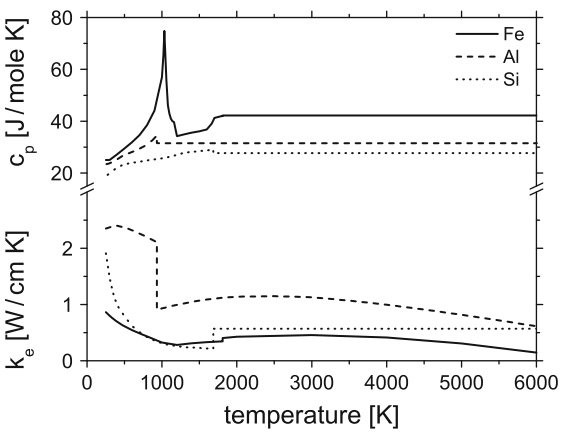

Fig. 3.2 Temperature dependence of the molar specific heat (*top*) and the thermal conductivity (*bottom*) of iron (*solid line*), aluminum (*dashed line*) and silicon (*dotted line*). Data from [70]

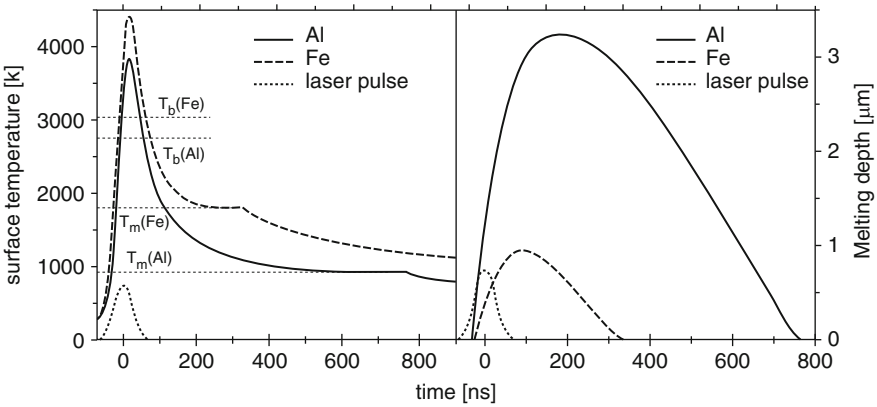

Fig. 3.3 Time evolution of the surface temperature profiles (*left*) and the melting depths (*right*) of the iron and the aluminum substrates irradiated at 4 J/cm^2. The melting and the boiling points of each element are indicated

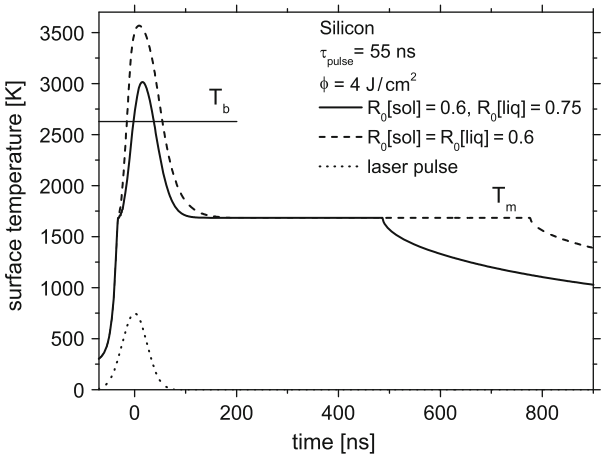

Fig. 3.4 Comparison between the Si surface temperature profiles obtained using temperature-dependent (*solid line*) and temperature-independent (*dashed line*) reflectivities

temperature-independent. In the case of the silicon substrate, the reflectivity of the solid is about 20% lower than the liquid (for near UV wavelength, $R_0(T < T_\mathrm{m}) \simeq 0.6$ and $R_0(T \geq T_\mathrm{m}) \simeq 0.75$ [61, 71, 72]) and different temperature profiles are obtained if the temperature dependence of R_0 is taken into account, as illustrated in Fig. 3.4. In particular, when the melting point is reached, the higher reflectivity of the liquid phase reduces the absorbed laser energy, leading to a decrease of the maximum surface temperature and of the melting time.

Powerful laser beams not only affect the intrinsic optical properties but also the surface topography (shape, roughness) of the irradiated material, which influences the beam-solid coupling. Surface corrugations are almost always related to melting

or evaporation. In particular, melting of a surface by a laser beam typically leaves its trace in form of ripples or corrugations. The patterns are often unrelated to the beam profile and they appear even if the beam is perfectly smooth [8].

3.5 Phenomena Occurring on the Target Surface

Although the temporal evolution of the temperature profiles and the related phase transformations *inside* the irradiated substrates have been described, important phenomena take place also *on* the surface of the target, as illustrated in the following sections.

3.5.1 Vaporization

According to the heat transport equation, the laser beam can be absorbed by the substrate causing melting and vaporization. In the case of strong evaporation, typically at fluences of several J/cm^2 with nanosecond pulse duration, the more proper boundary condition at the target surface would be to include also the velocity v_{ev} of the evaporation front. Using (3.28), we can write [61]:

$$v_{\mathrm{ev}} = \frac{j_{\mathrm{ev}}}{\rho} = \frac{p_{\mathrm{D}}(T)}{\rho\sqrt{(2\pi k_{\mathrm{B}} T/M_{\mathrm{a}})}} \tag{3.37}$$

In the reference frame attached to the liquid–vapor interface moving with velocity v_{ev}, the left-hand-side of the heat equation, (3.22), should be written as:

$$C_{\mathrm{L}}(T)\frac{\partial T(z,t)}{\partial t} \rightarrow C_{\mathrm{L}}(T)\left(\frac{\partial T(z,t)}{\partial t} - v_{\mathrm{ev}}\frac{\partial T(z,t)}{\partial z}\right). \tag{3.38}$$

Both cases of stationary and non-stationary evaporations can be treated with proper approximations [61], but the correct treatment should consider: (a) the hydrodynamic motion of the evaporated material, (b) the decrease of the vapor temperature due to its expansion, and (c) the backward flux of the evaporated species. The vaporized atoms/molecules leave the substrate at temperature T_{s} with half-Maxwellian non-equilibrium velocity distribution (the velocity is initially in the direction normal to the target surface). Due to the collisions with other atoms/molecules, the vapor propagates with hydrodynamic speed v_{v} and the velocity distribution becomes Maxwellian (i.e., in thermodynamical equilibrium) [73]. The transformation from non-equilibrium to equilibrium distributions takes place in a thin layer of few mean free paths called *Knudsen layer*, as sketched in Fig. 3.5.

The detailed mathematical analysis of the transformation was performed by Anisimov [74] with a proper definition of the velocity distribution and using the conservation of mass, momentum, and energy across the Knudsen layer. The results show that the temperature T_{v} of the vapor beyond the Knudsen layer is lower than T_{s},

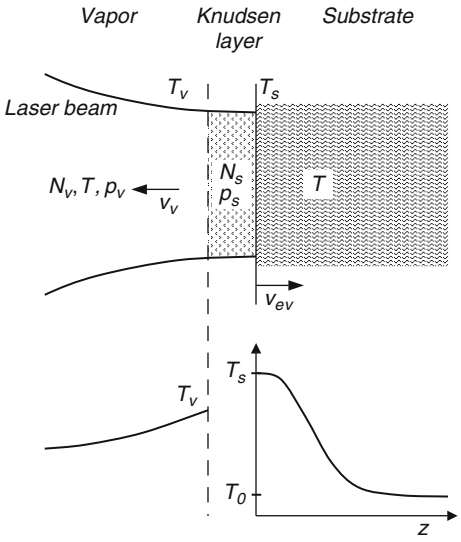

Fig. 3.5 Irradiation geometry (*top*) and temperature profiles within the target and the ambient medium (*bottom*): effect of the Knudsen layer

due to the partial transformation of thermal energy into kinetic energy of the expanding vapor plume. Besides, the number density of the vaporized species and the vapor pressure behind the Knudsen layer (subscript "*v*", i.e., vapor) can be related to the same values within the layer (subscript "*s*", i.e., surface) as follows:

$$\begin{aligned} T_\mathrm{v} &= T_\mathrm{s}(1 - 0.33\ \Pi); \\ N_\mathrm{v} &= N_\mathrm{s}(T_\mathrm{s})/(1 + 2.2\ \Pi); \\ p_\mathrm{v} &= N_\mathrm{v} k_\mathrm{B} T_\mathrm{v} = p_\mathrm{s}(T_\mathrm{s}) \frac{1 - 0.33\ \Pi}{1 + 2.2\ \Pi}, \end{aligned} \tag{3.39}$$

where the *Mach number* Π determines the expansion velocity v_v of the species beyond the Knudsen layer: in general $v_\mathrm{v} = \Pi c_\mathrm{s}$, where c_s is the speed of sound. For a vapor expanding in vacuum, $\Pi = 1$ [73], but if the laser irradiation takes place in a gaseous medium, Π (with $0 < \Pi < 1$) must be calculated theoretically or measured experimentally [61].

3.5.2 Recondensation

Using (3.39) and considering the vapor as an ideal gas, it can be verified that the vapor beyond the Knudsen layer is strongly supersaturated. In fact:

$$N_\mathrm{v} = N_\mathrm{s}(T_\mathrm{s})/(1 + 2.2\ \Pi) > N_\mathrm{s}(T_\mathrm{v}) = p_\mathrm{s}(T_\mathrm{v})/k_\mathrm{B} T_\mathrm{v}$$

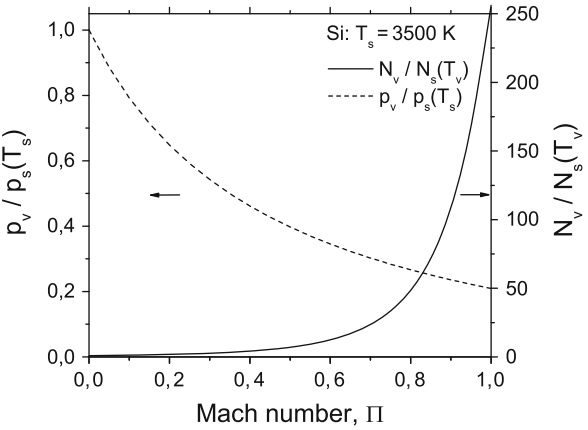

Fig. 3.6 Ratios of the vapor pressures within and beyond the Knudsen layer (*dashed line*) and the densities of the vaporized species obtained from the Anisimov analysis and from Clausius-Clapeyron equation (*solid line*) as a function of the Mach number for a silicon surface at 3,500 K

An example is reported in Fig. 3.6. The ratios $N_v/N_s(T_v)$ and $p_v/p_s(T_s)$ for a silicon target at $T_s = 3{,}500$ K are plotted as a function of the Mach number Π.

The supersaturation is always present ($N_v/N_s(T_v) > 1$), and it is much stronger for high values of Π (i.e., for low ambient pressures). Therefore, the recondensation of the evaporated species may start beyond the Knudsen layer. Besides, in the presence of a reactive atmosphere, the chemical reaction between the vapor and the ambient gas might lead to the formation and the subsequent condensation of chemical compounds. The pressure acting on the target surface is the pressure inside the Knudsen layer, that is the saturated vapor pressure p_s at the temperature T_s, given by the Clausius-Clapeyron equation (3.29). For silicon at $T_s = 3{,}500$ K, we have $p_s(T_s) \simeq 10^2$ bar. The dramatic effect of the surface temperature on the saturated vapor pressure is illustrated in Fig. 3.7: the surface temperature profiles of the silicon target already shown in Fig. 3.4 have been used to compute the vapor pressure vs. time according to the Clausius-Clapeyron equation.

A moderate increment of the surface temperature from 3,000 to 3,500 K leads to the enormous increase of the vapor pressure from 10 bar to almost 160 bar for a time interval comparable to the pulse duration ($\tau_{pulse} = 55$ ns).

3.5.3 Plasma Formation

When the laser irradiance is high enough ($\geq 10^9$ W/cm^2), the vapor or the ambient gas can become ionized, and properly described as a *plasma*. Within a gas at temperature T_g, the collisions between thermal electrons and vaporized species produce a certain degree of ionization given by the Saha equation [61]. The ionized

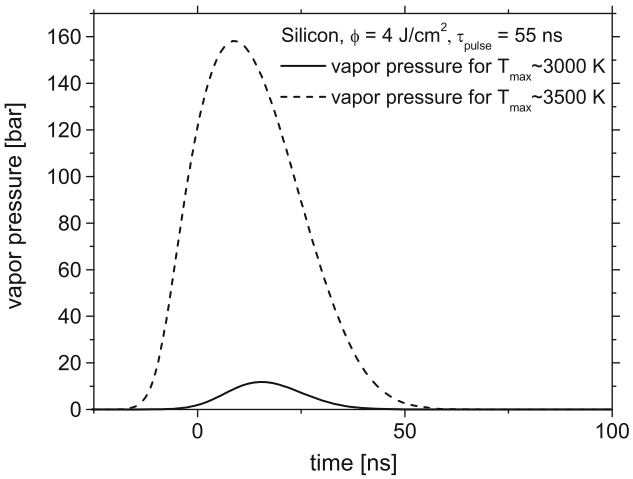

Fig. 3.7 Influence of the Si surface temperature on the saturated vapor pressure (the temperature profiles shown in Fig. 3.4 have been used to calculate the vapor pressures)

gas strongly absorbs the laser radiation and expands within the laser beam channel, thus shielding the substrate from the laser light. The propagating plasma is generally termed LSAW. If the LSAW moves with subsonic velocity with respect to the ambient medium, it is called laser-supported combustion wave (LSCW). As the laser intensity increases, the LSAW can exceed the sound speed becoming a laser-supported detonation wave (LSDW). The typical irradiance necessary to ionize a gas with a free propagating laser (i.e., without any target) is of the order of $10^9 - 10^{11}$ W/cm^2, but it can decrease by several orders of magnitude in front of a solid or liquid target [28, 61]. The theories of LSC and LSD waves have been developed in the Seventies [6, 75–77] obtaining quantitative evaluations of the propagation velocity of the wave front and the pressure behind it. In the case of LSC wave, the laser-light is absorbed within the plasma and dissipated in the ambient medium via heat conduction and thermal radiation. The energy balance can be written as [77]:

$$k^{\text{eff}} \Delta T/d = d(\alpha_{\text{p}} I_0 - J^{\text{loss}}), \tag{3.40}$$

where k^{eff} is an effective thermal conductivity, α_{p} is the absorption coefficient of the plasma, ΔT is the temperature jump across the LSC wave, d is the thickness of the wave front, I_0 is the laser irradiance, and J^{loss} is the volumetric energy loss [J/cm^3 s] of the plasma, due to radiation/conduction. Using the heat transport equation, we obtain [77]:

$$C_{\text{gas}} \frac{\partial T}{\partial t} = C_{\text{gas}} v_{\text{LSC}} \frac{\Delta T}{\Delta x} = v_{\text{LSC}} C_{\text{gas}} \frac{\Delta T}{d} = k^{\text{eff}} \frac{\Delta T}{d^2} \tag{3.41}$$

where C_{gas} is the specific heat of the hot gas, while v_{LSC} is the velocity of the wave front. Using (3.40) in (3.41) to eliminate d, the LSCW front velocity becomes [77]:

$$v_{\text{LSC}} = \frac{k^{\text{eff}}}{C_{\text{gas}}} \sqrt{\frac{\alpha_{\text{p}} I_0 - J^{\text{loss}}}{k^{\text{eff}} \Delta T}}. \tag{3.42}$$

For intense laser beams ($I_0 \gg J^{\text{loss}}/\alpha_{\text{p}}$), we have $v_{\text{LSC}} \propto I_0^{1/2}$ and typical values of $10 - 100$ m/s [28]. On the other hand, if $I_0 \approx J^{\text{loss}}/\alpha_{\text{p}}$, we have $v_{\text{LSC}} \approx 0$ and the LSCW becomes a stationary wave called *plasmatron* [78, 79]. If the velocity of the propagating wave exceeds the sound velocity of the medium, a supersonic LSD wave is produced. Treating such a wave as a hydrodynamic discontinuity, and using the conservation of mass, momentum and energy, its velocity can be estimated as [75]:

$$v_{\text{LSD}} = [2(\gamma^2 - 1) I_0/\rho_0]^{1/3} \propto I_0^{1/3}, \tag{3.43}$$

where γ is the adiabatic coefficient and ρ_0 is the mass density of the ambient gas. The gas pressure behind the wave is [75]:

$$p_{\text{LSD}} = \frac{\rho_0 \, v_{\text{LSD}}^2}{\gamma + 1} \propto I_0^{2/3}. \tag{3.44}$$

Even at moderate laser irradiance $I_0 \approx 10^8$ W/cm^2 and considering air in standard conditions ($\rho_0 \approx 1.3$ kg/m^3 and $\gamma \approx 7/5$) as a medium, we obtain $v_{\text{LSD}} \approx 10^4$ m/s and $p_{\text{LSD}} \approx 5 \times 10^2$ bar.

It is clear that in both cases of pure vaporization or plasma formation, the pressure acting on the target surface is of the order of 10^2 bar, and the melt can be heated well above the boiling point. Such high pressures acting on the surface might give rise to strong hydrodynamic motion (convection, piston effect) of the molten layer.

3.5.4 Laser Supported Absorption Waves

The vapor formed by intense laser irradiation plays an important role in laser material treatment. The range of irradiances where evaporation is achieved stretches from some 10^3 W/cm^2 to the highest realized irradiances of 10^{21} W/cm^2 [5, 80, 81]. It is clear that many physically distinct regimes are found in this enormous energy range. At relatively low irradiances (below 10^6 W/cm^2), the vapor is tenuous and essentially transparent, but with increasing irradiance it becomes supersaturated. Between roughly 10^7 and 10^{10} W/cm^2 and depending on the wavelength, the vapor becomes partially ionized and absorbs a substantial fraction of the laser energy. On the other hand, radiation re-emitted from the vapor plasma may heat the solid very efficiently [8].

If the vapor becomes ionized and absorbs part or all of the incident irradiation, the energy is converted into internal energy of the plasma, radiated away as

thermal radiation or consumed in hydrodynamic motion. This plasma forms close to the evaporating surface, and the temperature and degree of ionization depend on the incident irradiance. If an absorbing gas plasma has formed, an interesting effect is observed. The plasma expands from the surface and moves towards the incoming laser beam. Such a propagating plasma is called LSAW. LSA waves are generally divided into several regimes: Laser Supported Combustion (LSC), Laser Supported Detonation (LSD), and Laser Supported Radiation (LSR). All these and the related phenomena are extensively described theoretically in the literature [6, 8, 73, 75, 76, 82–87], but experimental results are rarely found. The two most important regimes are divided according to the propagation velocity of the plasma front, i.e., if the latter is subsonic or supersonic with respect to the gas. The weakly absorbing subsonic variation is called LSCW. The absorbing plasma heats and compresses the surrounding gas by expansion and thermal radiation until this hot and compressed gas itself becomes an absorbing plasma. Under these condition, the absorption front is moving towards the laser beam, because the metal surface is blocking its propagation in the opposite direction. For this case, a stationary plasma above the surface is formed. A similar behavior is valid for the LSD wave, except that there the plasma front is moving with supersonic velocity and the laser radiation if fully absorbed in the plasma front. The theory of LSC and LSD waves was formulated by Raizer [6], who calculated the plasma surface pressure (plasma pressure acting at the surface) caused by the LSD waves to be:

$$p_{\mathrm{s}}^{\mathrm{LSD}} = \frac{[2(\gamma^2-1)]^{2/3}}{\gamma+1}\left[\frac{\gamma+1}{2\gamma}\right]^{\frac{2\gamma}{\gamma-1}} \rho_0^{1/3} I_0^{2/3} \tag{3.45}$$

and the velocity of the LSD wave $v_{\mathrm{w}}^{\mathrm{LSD}}$ to be:

$$v_{\mathrm{w}}^{\mathrm{LSD}} = \left[2(\gamma^2-1)\frac{I_0}{\rho_0}\right]^{1/3}. \tag{3.46}$$

For the LSC wave [82, 83, 88] the surface pressure is:

$$p_{\mathrm{s}}^{\mathrm{LSC}} = \left[1-\frac{2W}{\gamma_0-1}\right]\left[\frac{\gamma_0+1}{2}\right]^{1/3}\left[\frac{(\gamma-1)(\gamma+1)}{(\gamma+W)(\gamma_0-1-2W)}\right]^{2/3} \rho_0^{1/3} I_0^{2/3}, \tag{3.47}$$

with W being a dimensionless particle velocity, $W = 0.009 \cdot I_0^{2/3}$ for I_0 in MW/cm^2. The wave velocity is:

$$v_{\mathrm{w}}^{\mathrm{LSC}} = (W+1)\left[\frac{2(\gamma-1)(\gamma_0-1)}{(\gamma_0+1)(\gamma+W)(\gamma_0-1-2W)} \cdot \frac{I_0}{\rho}\right]^{1/3} \tag{3.48}$$

where $\gamma_0 = 1.4$ and $\gamma = 1.2$ are the adiabatic exponents for the surrounding gas and the metal vapor, respectively.

For the irradiation with 4 J/cm^2, i.e., for an irradiance of 7.27×10^7 W/cm^2, taken as constant for 55 ns, a LSC pressure of $p_s^{LSC} = 48$ MPa is derived. This is in agreement with experimental results given by Schutte [89].

Reilly et al. [90] developed a model for the temporal behavior of the plasma pressure in a LSC wave. They estimated the time when the rarefaction fans from the sides and the top reaches the surface and thus lower the plasma surface pressure. For the modeling of the temporal behavior of the plasma pressure acting at the surface, Reilly et al. used a two-dimensional model [90], which takes into account the expansion of the plasma at its lateral borders. During expansion, zones with lowered pressures are formed, and they move inwards with the sound velocity c_S inside the plasma. The time τ_{2D}, which is needed by the lateral rarefaction fans to reach the center is given by:

$$\tau_{2D} = \frac{r_p}{c_S}, \tag{3.49}$$

where r_p is the radius of the laser spot (here assumed circular) and the sound velocity c_S is given by:

$$c_S^{LSC} = \left(\frac{\gamma \, p_s^{LSC}}{\rho_0} \right)^{1/2} \left[\frac{W+1}{W} \frac{\gamma_0 - 1}{\gamma_0 + 1} \right]^{1/2}. \tag{3.50}$$

A second rarefaction wave is starting when the laser pulse ends at time τ_p and the shock wave is no longer heated by the laser beam, but is still expanding and cooling. The rarefaction then needs the time τ_z:

$$\tau_z = \tau_p + v_w^{LSC} \tau_p / c_S^{LSC} \tag{3.51}$$

to reach the metal surface. In conclusion, the development of the plasma pressure $p_S(t)$ in time, acting at the surface, is characterized by the three times τ_p, τ_z, and τ_{2D}. If we assume a LSC wave, different cases have to be regarded, depending on the order of these times. For the present case with the values of $I = 72$ MW/cm^2, $\rho_0 = 1.25$ g/cm^3, $\gamma = 1.2$, and $\gamma_0 = 1.4$ a sound velocity of $c_S = 7,551$ m/s is obtained[1]. Taking the width of the laser spot as $r_p = 2$ mm, we obtain $\tau_{2D} = 265$ ns and from (3.51) follows $\tau_z = 113$ ns. Therefore, the times order as $\tau_p \leq \tau_z \leq \tau_{2D}$ and according to Reilly [90] the following behavior of the plasma surface pressure at the center of the laser spot is obtained:

$$t \leq \tau_z : p(t) = p_P \tag{3.52}$$

$$\tau_z \leq t \leq \tau_{2D} : p(t) = p_P \left(\frac{t}{\tau_z} \right)^{-2/3} \tag{3.53}$$

$$\tau_{2D} \leq t : p(t) = p(\tau_{2D}) \left(\frac{t}{\tau_{2D}} \right)^{-6/5}. \tag{3.54}$$

[1] Here, a constant laser irradiance over the 55 ns pulse duration is assumed.

It is important to note that the high pressures induced by the plasma waves is acting for times much longer than the laser pulse duration and also larger than the time the surface remains liquid.

3.6 Material Transport Phenomena

At laser molten metal surfaces, many mechanisms contribute to material transport phenomena, such as convection, evaporation, and hydrodynamic motions caused by temperature and pressure gradients [1, 8, 73, 91]. The pressures are produced by the evaporation itself (recoil pressure) or by the LSAW as discussed before. The most important mechanisms for lateral material transport in the liquid state are connected to the temperature dependence of the surface tension $\sigma(T)$ and the piston mechanism [1, 4]. Variations of the surface tension may arise from temperature gradients across the surface of the molten material. If this is due to an inhomogeneous laser intensity profile, this is called thermocapillary effect. An approximation of the radial component of this effect is given by Baeuerle [1],

$$v_{\mathrm{lat}} \approx \frac{d_{\mathrm{liq}} \Delta T}{\eta_{\mathrm{v}} d_p} \cdot \frac{\mathrm{d}\sigma}{\mathrm{d}T}, \tag{3.55}$$

where d_{liq} again is the melting depth, ΔT the lateral temperature difference, η_{v} the dynamic viscosity of the material, d_{p} the diameter of the laser spot and $\mathrm{d}\sigma/\mathrm{d}T$ the temperature dependence of the surface tension. An upper limit for the velocity v_{lat} as calculated with the values $\mathrm{d}\sigma/\mathrm{d}T = -5 \times 10^{-4}\,\mathrm{N/(m\,K)}$, $d_{\mathrm{p}} = 2\,\mathrm{mm}$, $d_{\mathrm{liq}} = 1\,\mu\mathrm{m}$, $\eta_v = 6.9 \times 10^{-3}\,\mathrm{Pa{\cdot}s}$ and $\Delta T = 4,700\,\mathrm{K}$, yields $v_{\mathrm{lat}} \approx 0.2\,\mathrm{m/s}$.

There are two other main mechanisms of material removal in the beam interaction zone: (a) melt ejection by the vaporization-induced recoil pressure and plasma pressure and (b) melt evaporation (high power or short pulses) [92]. At moderate temperatures above the melting temperature, the vaporization recoil and plasma pressure are the primary factors for the material transport out of the laser beam interaction zone under the regime of hydrodynamic flow. At higher surface temperature (higher fluences), the melt removal due to evaporation exceeds the hydrodynamic mechanism. The mechanisms of the propagation of the evaporation front were considered in detail by Anisimov and Khokhlov [73].

The vapor particles escaping from a hot surface have a Maxwellian velocity distribution corresponding to the surface temperature, but their velocity vectors all point away from the surface. This anisotropic distribution is brought to equilibrium within a few mean-free paths by atomic collisions (Knudsen layer) [86, 93–96]. Some of them are also scattered back to the surface and are then contributing to the recoil pressure [92], which is in the order of the saturated vapor pressure [73]. Beyond this Knudsen layer, the vapor reaches a new internal equilibrium with homogeneous velocity distribution, but with a different temperature. Poprawe [86] made

a detailed calculation of the recoil pressure p_r. For the irradiation with 4 J/cm^2, for example, we achieved $p_r = 2.9 \times 10^7$ Pa, when using his parameterizations.

As just discussed, a high plasma pressure and the recoil pressure are acting at the liquid surface inside the laser spot of length a and width b. This pressure difference to the ambient pressure Δp is acting as a piston and moves material from the center through the sides out of the melt pool. This causes a lowering of the surface by the piston.

The problem was treated by von Allmen [4, 8] and also by Luft et al. [97] for pulsed laser drilling. They assumed a non-viscous and incompressible melt and the pressure distribution was approximated by a " top hat" profile with pressure $p_0 + \Delta p$ inside the laser spot of radius r_p and ambient pressure p_0 outside. Then, the radial velocity of the melt extraction follows from the volume work:

$$v_{lat} = \sqrt{\frac{2\Delta p}{\rho}} \tag{3.56}$$

where ρ is the density of the liquid ($\rho = 7$ g/cm^3) and Δp is the pressure difference which is given by the sum of plasma pressure and recoil pressure $\Delta p = p_p + p_r$. With $p_r = 2.9 \times 10^7$ Pa and $p_p = 4.8 \times 10^7$ Pa, this yields $v_{lat} = 148$ m/s, which has to be compared to a lateral velocity $v_r \approx 0.2$ m/s, induced by the Marangoni convection [1]). Thus, the piston mechanism should be the dominant mechanism for the lateral material transport.

The liquid escapes through the perimeter of the melt pool and if the two streams of melt extraction and new laser melting are in a stationary state, i.e., u is describing the velocity of the lowering piston, by assuming a rectangular laser spot with dimensions $a \times b$ and the pressure being constant inside the laser spot, we obtain:

$$\dot{V}_{lat} = \dot{V}_{pist} \Leftrightarrow 2(a+b)\, d_{liq}\, \rho\, v_{lat} = a\, b\, \rho\, u. \tag{3.57}$$

The thickness of the melt d_{liq} was estimated [8] to be:

$$d_{liq} = \frac{k}{u} \ln\left(\frac{T_b}{T_m}\right), \tag{3.58}$$

so that for the velocity of the piston movement u follows:

$$u = \sqrt{\frac{2(a+b)\, k\, \ln(T_b/T_m)}{a \cdot b}} \cdot \left(\frac{2\Delta p}{\rho}\right)^{1/4}. \tag{3.59}$$

Since the numerical simulation for the melting depth d_{liq} has been performed, it is much more accurate to use this for the calculation of the piston effect. From (3.57), we can extract the following expression for the total piston movement or surface lowering Δz^{pist} during the laser pulse:

$$\Delta z^{pist} = \int_0^{t_{liq}} \frac{2 \cdot (a+b) \cdot d_{liq}(t)}{a \cdot b} \cdot \sqrt{\frac{2\Delta p}{\rho}}\, \mathrm{d}t. \tag{3.60}$$

For example by using $\rho = 7\,\mathrm{g/cm^3}$, area $A = a \times b = 2 \times 3\,\mathrm{mm^2}$ and a pressure difference $\Delta p = (4.8 + 2.9) \times 10^7\,\mathrm{Pa}$, we calculate for $\phi = 4\,\mathrm{J/cm^2}$ with the simulation given above a piston effect of $\Delta z^{\mathrm{pist}} = 12(4)\,\mathrm{nm/pulse}$.

Also turbulences or bifurcations may play an important role for a fast material transport. During carburizing of iron by irradiation with a CO_2 laser in propane, carburized layers of about $d \approx 10\,\mu\mathrm{m}$ have been found, where the thickness and homogeneity of these layers could not be explained with diffusion in the liquid state alone [98]. Also during the nitrification of Ti by irradiation with an ns excimer laser in nitrogen atmosphere, a significant influence of turbulences for the transport of the nitrogen is expected [99, 100]. These turbulences in the liquid surface may evolve from pressure gradients, produced by local changes in the plasma density or the temperature [101]. The number of turns of a turbulence during irradiation is approximated [101, 102] via the lateral material velocity v_{lat} and the pulse duration τ_{p}. It follows a traveling distance $\Delta s = v_{\mathrm{m}}\tau$ for a surface element. The lateral extension a_{bifurc} of the bifurcation is approximated by the periodicity of the structures at the surface after the irradiation [98,102]. As an example, for a velocity of $v_{\mathrm{lat}} = 124\,\mathrm{m/s}$ and with $\tau_{\mathrm{p}} = 55\,\mathrm{ns}$, a moving distance of $\Delta s = 12\,\mu\mathrm{m}$ is approximated.

3.7 Conclusions

The chapter shows the fundamental physical processes taking place during irradiation of materials with lasers. Heating and vaporization have been explained in relation to interaction times and have been calculated by means of heat transfer modeling and the Knudsen layer model. Lattice dynamics, electron-phonon coupling, phase transitions, and electromagnetic wave propagation have been described and related to the material properties. Plasma development and the formation of shock waves were shown too. The describing formulation offers additional information about reacting pressure induced forces and recondensation effects. Transport phenomena like convection or melt ejection (Piston effect) have been explained as well. Summarized, the chapter gives a detailed insight into the physics occurring during laser material interaction.

Acknowledgements A significant part of this work was financially supported by the Deutsche Forschungsgemeinschaft (grants DFG Scha 632/3, /4, /9, /10, and /11), which is gratefully acknowledged.

References

1. D. Bäuerle, *Laser Processing and Chemistry*. Springer Series in Materials Science (Springer, Berlin, 1996)
2. J.F. Ready, J. Appl. Phys. **36**, 462 (1965)
3. J.F. Ready, *Effects of High-Power Laser Radiation* (Academic, New York, 1971)
4. M. von Allmen, J. Appl. Phys. **47**, 5460 (1976)

5. M. von Allmen, *Laser Beam Interactions with Materials*, *Springer Series in Materials Science*, vol. 2. (Springer, Berlin, 1987)
6. Y.P. Raizer, Sov. Phys. JEPT **31**, 1148 (1970)
7. D. Bäuerle, *Chemical Processing with Lasers*. Springer Series in Materials Science (Springer, Berlin, 1986)
8. M. von Allmen, A. Blatter, *Laser-Beam Interactions with Materials*. Springer Series in Materials Sciences (Springer, Berlin, 1994)
9. A. Einstein, Physikal. Zeitschrift **18**, 121 (1917)
10. T.H. Maimann, Nature **187**, 493 (1960)
11. M. Bertolotti (ed.), *Physical Processes in Laser-Materials Interactions*. (Plenum, New York, 1983)
12. M. Bass (ed.), *Laser Materials Processing*, *Materials processing – Theory and Practices*, vol. 3. (North Holland Publishing Company, Amsterdam, 1983)
13. B.L. Mordike (ed.), *Laser treatment of materials, Proc. 1st European Conference on Laser Treatment of Materials, ECLAT 1986, Bad Nauheim, Germany* (DGM Informationsgesellschaft, Oberursel, 1987)
14. W. Waidelich (ed.), *Laser, Optoelektronik in der Technik, Proc. 8. International Congress 'LASER87', München, Germany* (Springer, Berlin, 1987)
15. H. Sossenheimer, G. Sepold (eds.), *Proc. 2nd European Conference on Laser Treatment of Materials, ECLAT 1988, Bad Nauheim, Germany* (DVS-Verlag, Düsseldorf, 1988)
16. H.W. Bergmann, R. Kupfer (eds.), *Proc. 3rd European Conference on Laser Treatment of Materials, ECLAT 1990, Erlangen, Germany* (Sprechsaal Publishing Group, Coburg, 1990)
17. H. Gobrecht, *Optik*, *Bergmann-Schäfer: Lehrbuch der Experimentalphysik*, vol. 3. (Verlag Walter de Gruyter, Berlin, 1978)
18. K. Tradowski, *Laser: Grundlagen, Technik, Anwendungen* (Vogel-Verlag, Würzburg, 1979)
19. H. Weber, G. Herziger, *Laser – Grundlagen und Anwendungen* (Physik-Verlag, Weinheim, 1979)
20. F.K. Kneubühl, M.W. Sigrist, *Laser* (Teubner Taschenbücher Physik, Stuttgart, 1995)
21. H.W. Bergmann, S.Z. Lee, Opto Elektronik Magazin **3**, 623 (1987)
22. O. Svelto, *Principles of Lasers* (Springer, New York, 1998)
23. M. Bass, in *Laser Materials Processing*, *Materials processing – Theory and Practices*, vol. 3 ed. by Bass (North Holland Publishing Company, Amsterdam, 1983), chap. 1, pp. 1–14
24. I.J. Spalding, in *Physical Processes in Laser-Materials Interactions*. ed. by (Plenum, New York, 1983), pp. 1–47
25. T. Manzur, T. de Maria, W. Chen, C. Roychoudhuri, Proc. SPIE **2703**, 490 (1996)
26. U. Sowada, H.J. Kahler, D. Basting, World Lasers Almanac **1**, 50 (1988)
27. K.J. Schmatjko, G. Endres, World Lasers Almanac **1**, 46 (1988)
28. M. von Allmen, A. Blatter, *Laser-Beam Interactions with Materials.* (Springer, Berlin, 1998)
29. N.W. Ashcroft, N.D. Mermin, *Solid State Physics.* (Saunders College, Philadelphia, 1976)
30. D. Pines, P. Nozières, *The Theory of Quantum Liquids.* (Benjamin, New York, 1966)
31. M. Wolf, T. Hertel, E. Knoesel, G. Ertl, Phys. Rev. Lett. **76**, 535 (1996)
32. R. Burgermeister, M. Aeschlimann, R. Knorren, K.H. Bennemann, Phys. Rev. B **61**, 9427 (2000)
33. G. Grimvall, *The Electron–Phonon Interaction in Metals* (North-Holland, Amsterdam, 1981)
34. P.B. Allen, Phys. Rev. Lett. **59**, 1460 (1987)
35. P.B. Allen, Phys. Rev. B **36**, 2920 (1987)
36. B.L. Kapeliovich, S.I. Anisimov, T.L. Perel'man, Sov. Phys. JETP **39**, 375 (1975)
37. L.H. Acioli, E.P. Ippen, C.-K. Sun, F. Vallée, J.G. Fujimoto, Phys. Rev. B **50**, 15337 (1994)
38. R. Sprik, R.H.M. Groeneveld, A. Lagendijk, Phys. Rev. B **51**, 11433 (1995)
39. D. Bejan, G. Raşeev, Phys. Rev. B **55**, 4250 (1997)
40. V.E. Gusev, O.B. Wright, Phys. Rev. B **57**, 2878 (1999)
41. A.V. Lugovskoy, I. Bray, Phys. Rev. B **60**, 3279 (1999)
42. M. Achermann, S. Tzortzakis, D. Christofilos, N. Del Fatti, C. Voisin, F. Vallée, Phys. Rev. B **61**, 16956 (2000)

43. M. Vicaneck, B. Rethfeld, A. Kaiser, G. Simon, Phys. Rev. B **65**, 214303 (2002)
44. M. Lisowski, P.A. Loukakos, U. Bovensiepen, J. Stähler, C. Gahl, M. Wolf, Appl. Phys. A **78**, 165 (2004)
45. E. Carpene, Phys. Rev B **74**, 024301 (2006)
46. A. Daunois, E. Beaurepaire, J.-C. Merle, J.Y. Bigot, Phys. Rev. Lett. **76**, 4250 (1996)
47. I.M. Lifshitz, M.I. Kaganov, L.V. Tanatarov, Sov. Phys. JETP **4**, 173 (1957)
48. C. Kittel, *Introduction to Solid State Physics* (Wiley, New York, 1971)
49. S. Funk, M. Wolf, S.S. Wellershoff, M. Bonn, D. N. Denzler, J. Hohlfeld, Phys. Rev. B **61**, 1101 (2000)
50. CRC, *Handbook of Chemistry and Physics, 63 rd. Edition* (CRC, Boca Raton, 1982/1983)
51. J.R. Bettis, Appl. Opt. **31**, 3448 (1992)
52. V. Letokhov, Appl. Phys. B Lasers Opt. **46**(3), 237 (1988)
53. D. von der Linde, K. Sokolowski-Tinten, J. Bialkowski, Appl. Surf. Sci. **109–110**, 1 (1997)
54. C. Chou, S. Polyakov, A. Kuzmich, H. Kimble, Phys. Rev. Lett. **92**(21), 213601 (2004)
55. T. Mayer-Kuckuk, *Atomphysik* (BG Teubner, Stuttgart, 1997)
56. M.F. Allmen, in *Physical Processes in Laser-Materials Interactions*, ed. by M. Bertolotti (Plenum, New York, 1983) chap. 2, pp. 49–75
57. P. Grosse, *Freie Elektronen in Festkörpern.* (Springer, Berlin, 1979)
58. G.E.R. Schulze, *Metallographie.* (Springer, Wien-New York, 1974)
59. W. Amende, *Härten von Werkstoffen und Bauteilen des Maschinenbaus mit dem Hochleistungslaser*. Technologie Aktuell 3 (VDI-Verlag, Düsseldorf, 1985)
60. J.D. Jackson, *Klassische Elektrodynamik.* (Verlag Walter de Gruyter, Berlin, 1983)
61. D. Bäuerle, *Laser Processing and Chemistry* (Springer, Heidelberg, 2000)
62. V.G. Gregson, in *Laser Materials Processing*, *Materials processing – Theory and Practices*, vol. 3, ed. by Bass (North Holland Publishing Company, Amsterdam, 1983), chap. 4, pp. 201–233
63. H.F. Mark (ed.), *Encyclopedia of Chemical Technology / Kirk-Othmer* (Wiley, New York, 1978)
64. C.A.J. Fletcher, *Computational Techniques for Fluid Dynamic 1.* (Springer, Berlin, 1988)
65. S. Fähler, H.U. Krebs, Appl. Surf. Sci. **96–98**, 61 (1996)
66. C. Illgner, P. Schaaf, K.P. Lieb, R. Queitsch, J. Barnikel, J. Appl. Phys. **83**(6), 2907 (1998)
67. C. Illgner, Untersuchungen zum Lasernitrieren von Eisen. Ph.D. thesis, Universität Göttingen, Göttingen (1997)
68. F. Landry, Lasernitrieren von Armco-eisen und Eisenwerkstoffen. Ph.D. thesis, Universität Göttingen, Göttingen (1999)
69. E. Carpene, P. Schaaf, Phys. Rev. B **65**, 224111 (2002)
70. Y.S. Touloukian, C.Y. Ho (eds.), *Thermophysical Properties of Matter*, vol. 1 and 4. (Plenum, New York, 1970)
71. S. Higashi, T. Sameshima, Jpn. J. Appl. Phys. **40**, 480 (2001)
72. M. Hatano, S. Moon, M. Lee, K. Suzuki, C.P. Grigoropoulos, J. Appl. Phys. **87**, 36 (2001)
73. S.I. Anisimov, V.A. Khokhlov, *Instabilities in Laser-Matter Interaction.* (CRC, Boca Raton, London, Tokyo, 1995)
74. S.I. Anisimov, Sov. Phys. JETP **27**, 182 (1968)
75. Y.P. Raizer, Sov. Phys. JETP **21**, 1009 (1965)
76. A. Pirri, Phys. Fluids **16**, 1435 (1973)
77. A.A. Boni, F.Y. Su, Phys. Fluids **17**, 340 (1974)
78. Y.P. Raizer, Sov. Phys. Usp. **23**, 789 (1980)
79. Y.P. Raizer, Sov. Phys. Quantum Electron. **14**, 40 (1984)
80. B.N. Chichkov, C. Momma, S. Nolte, F.V. Alvensleben, A. Tünnermann, Appl. Phys. A **63**, 109 (1996)
81. G. Marowsky, C.K. Rhodes, Appl. Phys. B **66**, 475 (1998)
82. A.N. Pirri, R.C. Root, P.K.S. Wu, AIAA J. **16**, 1296 (1978)
83. A.A. Boni, F.Y. Su, P.D. Thomas, H.M. Musal, Theoretical study of laser-target interactions. Final Tech. Report SAI 77-77-567-LJ, Science Application Inc., La Jolla, California (1977)
84. L.I. Sedov, *Similarity and Dimensional Methods in Mechanics* (Academic, New York, 1959)

85. N. Ferriter, D.E. Maiden, A.M. Winslow, J.A. Fleck, AIAA J. **5**, 1597 (1977)
86. R. Poprawe, Materialabtragung und Plasmaformation im Strahlungsfeld von UV-Lasern. Dissertation, Technische Hochschule Darmstadt (1984)
87. B.S. Holmes, C. Tarver, D.C. Ehrlich, H.E. Lindberg, The mechanical loads from LSD waves and their simultation. Final Report F29601-74-C-0051, Stanford Research Institute (1976)
88. R.G. Root, in *Laser-Induced Plasmas and Applications*, eds. by L.J. Radziemski, D.A. Cremers (Marcel Dekker Inc., New York, 1992)
89. K. Schutte, Prozessdiagnostik und technologische Untersuchungen zur Materialbearbeitung mit Excimerlasern. Ph.D. thesis, Universität Erlangen-Nürnberg, Nürnberg (1993)
90. J.P. Reilly, A. Ballantyne, J.A. Woodroffe, AIAA J. **17** (10), 1098 (1979)
91. H. Ishiguro, K. Ohyama, H. Nariai, T. Teramoto, J. Nucl. Sci. Technol. **27**(12), 1115 (1990)
92. V. Semak, A. Matsunawa, J. Phys. D: Appl. Phys. **30**, 2541 (1997)
93. R. Kelly, R.W. Dreyfus, Nucl. Instr. Methods B **32**, 341 (1988)
94. R. Kelly, J.E. Rothenberg, Nucl. Instr. Methods B **7/8**, 755 (1985)
95. R. Kelly, A. Miotello, B. Braren, C.E. Otis, Appl. Phys. Lett. **60** (24), 2980 (1992)
96. R. Bellantone, Y. Hahn, J. Appl. Phys. **78**, 1436 (1994)
97. A. Luft, U. Franz, A. Emsermann, J. Kaspar, Appl. Phys. A **63**, 93 (1996)
98. V.N. Anisimov, V.Y. Baranov, L.A. Bolshov, A.I. Ilyin, C.V. Kopetskii, V.S. Kraposhin, D.D. Malyuta, L.A. Matveeva, V.D. Pismennyi, A.Y. Sebrant, Phys. Chem. Mech. Surf. **3** (9), 2756 (1985)
99. E. D'Anna, G. Leggieri, A. Luches, Thin Solid Films **218**, 219 (1992)
100. I.N. Mihailescu, N. Chitica, L.C. Nistor, M. Popescu, V.S. Teodorescu, I. Ursu, A. Andrei, A. Barborica, A. Luches, M. Luisa de Giorgi, A. Perrone, B. Dubreuil, J. Hermann, J. Appl. Phys. **74**, 5781 (1993)
101. V.N. Anisimov, R.V. Arutyunyan, V.Y. Baranov, L.A. Bolshov, E.P. Velikhov, V.A. Dolgov, A.I. Ilyin, A.M. Kovalevich, V.S. Kraposhin, D.D. Malyuta, L.A. Matveeva, V.S. Mezhevov, V.D. Pismennyi, A.Y. Sebrant, Y.Y. Stepanov, M.A. Stepanova, Appl. Opt. **23**, 18 (1984)
102. E. D'Anna, G. Leggieri, A. Luches, M. Martino, A.V. Drigo, I.N. Mihailescu, S. Ganatsios, J. Appl. Phys. **69**, 1687 (1991)